

Alfvénic reacceleration of relativistic particles in galaxy clusters in the presence of secondary electrons and positrons

G. Brunetti,¹ P. Blasi²

¹ *INAF/Istituto di Radioastronomia, via Gobetti 101, I-40129 Bologna, Italy*

² *INAF/Osservatorio Astrofisico di Arcetri, Largo E. Fermi 5, I-50125 Firenze, Italy*

21 October 2018

ABSTRACT

In a previous paper (Brunetti et al. 2004) we presented the first self-consistent calculations of the time-dependent coupled equations for the electrons, hadrons and Alfvén waves in the intracluster medium, which describe the stochastic acceleration of the charged particles and the corresponding spectral modification of the waves. Under viable assumptions, this system of mutually interacting components was shown to accurately describe several observational findings related to the radio halos in clusters of galaxies.

In this paper, we add to the self-consistency of the calculations by including the generation and re-energization of secondary electrons and positrons, produced by the inelastic interactions of cosmic rays with the thermal gas in the intracluster medium. The bulk of Cosmic rays is expected to be confined within the cluster volume for cosmological times, so that the rate of production of secondary electrons, as well as gamma rays, may become correspondingly enhanced. If MHD waves are present, as it may be expected in the case of a recent merger event, then the reacceleration of secondary electrons and positrons can significantly affect the phenomenology of the non thermal processes in clusters. We investigate here these effects for the first time.

Key words: acceleration of particles - turbulence - radiation mechanisms: non-thermal - galaxies: clusters: general - radio continuum: general - X-rays: general

1 INTRODUCTION

The intracluster medium contains a non thermal component in the form of magnetic fields and relativistic particles, as demonstrated mainly by the appearance of diffuse radio emission (e.g., Feretti, 2003) and by studies of the rotation measure of radio sources in galaxy clusters (e.g., Clarke et al., 2001), but also by the hard X-ray (HXR) excess detected in a few galaxy clusters by the BeppoSAX and RXTE satellites (Fusco-Femiano et al. 2003; Rephaeli & Gruber 2003). While the radio radiation is certainly the result of synchrotron emission of high energy electrons in the intracluster magnetic field, HXRs may be explained in terms of inverse Compton scattering (ICS) of the same electrons off the photons of the cosmic microwave background (CMB), or as a result of bremsstrahlung emission from supra-thermal electrons (e.g., Ensslin, Lieu, Biermann 1999; Blasi 2000; Dogiel 2000; Sarazin & Kempner 2000). The latter solution does however require an energy input which may be supported only for a time shorter than a few hundred million years, otherwise the gas is overheated (Petrosian 2001; Blasi

2000). It should be mentioned that the rather poor sensitivity of the present and past facilities for the observation of HXRs does not allow to obtain a iron-clad detection of HXR excesses. Future observatories (e.g. ASTRO-E2, NEXT) are necessary to confirm (or disprove) the existence of these excesses (see Rossetti & Molendi 2004; Fusco-Femiano et al. 2004).

So far the most serious problem from the theoretical point of view is to identify the origin of the radiating high energy electrons. Buote (2001) and Schuecker et al. (2001) have found hints of a correlation between the non thermal diffuse radio emission and the presence of merger activity in the host clusters. This may indicate a link between the process of formation of galaxy clusters and the origin of the non thermal activity.

Two main avenues have been identified to explain the fact that such high energy electrons are present and able to radiate on distance scales larger than their typical loss lengths: in the context of the so-called *primary* models electrons are accelerated at shock waves through the first order

Fermi mechanism or they are continuously re-energized *in situ* on their way out (Jaffe 1977); the latter case is also called *reacceleration* model. On the other hand, in the context of *secondary electron* models electrons are secondary products of the hadronic interactions of cosmic rays with the intracluster medium, as first proposed by Dennison (1980).

Shock waves are unavoidably formed during merger events due to the supersonic relative motion of two (or more) infalling clusters. Since electrons have a short pathlength due to IC losses, they can only move a short distance away from the acceleration regions. If this acceleration site were to be at a shock front, the emission from the electrons would be concentrated around the shock rim (e.g., Miniati et al. 2001) and the spectrum of the radiation would be quite steep because of the low Mach numbers in the central virialized regions of clusters (Gabici and Blasi 2003, Berrington and Dermer 2003), where the radio emission is observed to come from. On the other hand, strong shocks are formed in the outskirts of clusters, and they may be responsible for the acceleration of protons (Ryu et al. 2003). These protons can then be advected into the cluster and there be confined for cosmological time scales (Völk et al. 1996; Berezhinsky, Blasi & Ptuskin 1997). The confinement unavoidably increases the energy density of cosmic rays in the intracluster medium, and may correspondingly favour the generation of gamma rays through the decay of neutral pions and of electrons and positrons through the decay of charged pions.

The origin of the emitting particles is still matter of debate (e.g., Ensslin 2004). The different models for the production of the radiating electrons have however a substantial predictive power, which can be used to discriminate among such models by comparing their predictions with observations. Recently Brunetti (2004) and Blasi (2004) have discussed at length the strong and the weak points of the models in explaining the phenomenology of existing data. Although the role of future observations remains crucial in order to achieve a definite conclusion of the right descriptions of the non thermal phenomena we detect, both authors concluded that, at least as far as the Coma cluster and few other well studied clusters are concerned, present data seem to suggest the presence of particle–reacceleration mechanisms active in the ICM. On the other hand, several complex and poorly understood processes are involved in these models.

Cluster mergers induce large-scale bulk flows with velocities $\sim 1000 \text{ km s}^{-1}$ or larger. These flows drive instabilities on large-scales which redistribute the energy of the mergers through the cluster volume and decay into turbulent velocity fields. It has been shown that reacceleration of a population of relic electrons by turbulence powered by cluster mergers is a promising mechanism to explain the very large scale of the observed radio emission, the complex spectral behaviour observed in some diffuse radio sources (Brunetti et al., 2001; Petrosian 2001; Ohno, Takizawa and Shibata 2002; Fujita, Takizawa and Sarazin 2003), and the observed occurrence of radio halos with cluster mass (Cassano & Brunetti 2005).

A step forward in the study of particle acceleration in galaxy clusters has been achieved by recent studies of the interaction between particles and Alfvén waves in a very general situation in which relativistic electrons, thermal protons and relativistic protons are present in the cluster vol-

ume (Brunetti et al., 2004, hereafter Paper I). In Paper I the interaction of all these components with the waves, as well as the turbulent cascading and damping processes of Alfvén waves, have been treated in a fully time-dependent way in order to calculate the spectra of electrons, protons and waves at any fixed time. This represented the first attempt to include in a self-consistent way hadronic cosmic rays in the reacceleration scenario. It was found there that radio halos and HXR tails could be activated for a time scale of $\sim 0.5 - 1$ Gyr through resonant interaction of particles with short-wavelength Alfvén waves, coming from the decay of merger induced turbulence. The role of the hadrons was found to be that of exerting a substantial backreaction, so that the non thermal activity is suppressed if the energy content in the form of hadrons gets larger than a few percent of the thermal energy. We named this phenomenon *wave-proton boiler*.

The present paper serves as a completion of the effort started in Paper I: here we add to the previous calculation the effect of the reacceleration of those electrons and positrons that are generated at any time as secondary products of the inelastic interactions of the confined cosmic rays with the thermal gas.

In Sections 2 and 3 we provide the reader with a review of the main aspects of the calculations developed in Paper I. In Section 4 we describe the general scenario in which secondary reaccelerated electrons are present. The application of the full calculation to the phenomenology of a Coma-like cluster is presented in Section 5. We conclude in Section 6.

2 PARTICLE ACCELERATION AND ENERGY LOSSES IN THE ICM

In this Section we briefly summarize the rates of energy loss and gain for non thermal leptons and protons in the intracluster medium, relying on the formalism already introduced in Paper I.

2.1 Energy losses for leptons

Four channels dominate the energy losses of relativistic leptons with momentum p , namely ionization, Coulomb scattering, synchrotron emission and IC. The rate of losses due to the combination of ionization and Coulomb scattering can be written following (Sarazin 1999):

$$\left(\frac{dp}{dt}\right)_i = -3.3 \times 10^{-29} n_{\text{th}} \left[1 + \frac{\ln(\gamma/n_{\text{th}})}{75} \right] \quad (1)$$

where n_{th} is the number density of the thermal plasma. The rate of synchrotron plus IC losses is:

$$\left(\frac{dp}{dt}\right)_{\text{rad}} = -4.8 \times 10^{-4} p^2 \left[\left(\frac{B_{\mu G}}{3.2}\right)^2 \frac{\sin^2 \theta}{2/3} + (1+z)^4 \right] \quad (2)$$

where $B_{\mu G}$ is the magnetic field strength in units of μG , and θ is the pitch angle of the emitting leptons; in case of efficient isotropization of the electron momenta, the $\sin^2 \theta$ is averaged to $2/3$. In the typical conditions of the ICM, radiative losses are dominant for leptons with Lorentz factor $\gamma \gg 100$, while Coulomb losses dominate at lower energies (Sarazin 1999,2002; Brunetti 2003).

2.2 Energy losses for protons

For relativistic protons, the main channel of energy losses in the ICM is provided by inelastic proton-proton collisions. The time-scale associated with this process is:

$$\tau_{pp} = \frac{1}{n_{\text{th}} \sigma_{pp} c} \sim 10^{18} \left(\frac{n_{\text{th}}}{10^{-3}} \right)^{-1} \text{ s}. \quad (3)$$

Thus inelastic pp scattering is weak enough to allow the accumulation of protons over cosmological times (Berezinsky, Blasi and Ptuskin 1997), however it is also efficient enough for the continuous production of pions, which in turn decay into gamma rays (for neutral pions), electron-positron pairs and neutrinos (for charged pions). The process of pion production in pp scattering is a threshold reaction that requires protons with kinetic energies larger than about 300 MeV.

For trans-relativistic and mildly relativistic protons, energy losses are dominated by ionization and Coulomb scattering. Protons more energetic than the thermal electrons, namely with $\beta_p > \beta_c \equiv (3/2m_e/m_p)^{1/2} \beta_e$ ($\beta_e \simeq 0.18(T/10^8 \text{ K})^{1/2}$ is the velocity of the thermal electrons), are affected by Coulomb interactions. Defining $x_m \equiv \left(\frac{3\sqrt{\pi}}{4} \right)^{1/3} \beta_e$, one has (Schlickeiser, 2002):

$$\frac{dp}{dt} \simeq -1.7 \times 10^{-29} \left(\frac{n_{\text{th}}}{10^{-3}} \right) \frac{\beta_p}{x_m^3 + \beta_p^3} \text{ cgs units}, \quad (4)$$

which has the following asymptotic behaviour :

$$\frac{dp}{dt} \propto \left(\frac{n_{\text{th}}}{10^{-3}} \right) \times \begin{cases} p & \text{for } mc\beta_c < p < mcx_m \\ p^{-2} & \text{for } mcx_m < p \ll mc \\ \text{Const.} & \text{for } p \gg mc \end{cases} \quad (5)$$

2.3 Alfvénic acceleration of relativistic particles

Different coupling between particles and waves may result in energy transfer from magnetic fluctuations into relativistic particles: Magneto-Sonic (MS) waves, magnetic Landau damping (Kulsrud & Ferrari 1971; Schlickeiser & Miller 1998), Lower Hybrid (LH) waves (e.g., Eilek & Weatherall 1999) and Alfvén waves are a few examples that have been investigated in the literature. Alfvén waves efficiently couple with relativistic particles via resonant interaction and they are likely to transfer most of their energy directly into these relativistic particles.

The resonant condition for a wave of frequency ω and wavenumber projected along the magnetic field k_{\parallel} , for a particle of species α with energy E_{α} and projected velocity $v_{\parallel} = v\mu$ is (Melrose 1968; Eilek 1979):

$$\omega - \nu \frac{\Omega_{\alpha}}{\gamma} - k_{\parallel} v_{\parallel} = 0, \quad (6)$$

where, in the quasi parallel case ($k_{\perp} \ll m_{\alpha} \Omega_{\alpha} / p$), $\nu = -1$ ($\nu = 1$) for electrons (protons and positrons).

The dispersion relation for Alfvén waves in an isotropic plasma with both thermal and relativistic particles was given by Barnes & Scargle (1973). In the conditions typical of galaxy clusters, the dispersion relation of Alfvén waves reduces to $\omega \simeq |k_{\parallel}| v_A$. Combining the dispersion relation of the waves with the resonant condition, Eq. 6, one can derive the resonant wavenumber, k_{res} , for a given momentum, $p = mv\gamma$, and angle, μ , of the particles :

$$k_{res} \sim |k_{\parallel}| = \frac{\Omega m}{p} \frac{1}{\left(\mu \pm \frac{v_A}{v} \right)}, \quad (7)$$

where the upper and lower signs refer to protons (and positrons) and electrons respectively. The interaction of particles with Alfvén waves can be thought of as a diffusion process in the momentum space of the particles. If the distributions of waves and particles are assumed to be isotropic, then the diffusion coefficient was found by Eilek & Henriksen (1984) to be:

$$D_{pp}(p, t) = \frac{2\pi^2 e^2 v_A^2}{c^3} \int_{k_{min}}^{k_{max}} \frac{W_k(t)}{k} \left[1 - \left(\frac{v_A}{c} \mp \frac{\Omega m}{pk} \right)^2 \right] dk, \quad (8)$$

where the minimum wavenumber (maximum scale length) of the waves interacting with particles with given momentum is:

$$k_{min} = \frac{\Omega m}{p} \frac{1}{\left(1 \pm \frac{v_A}{v} \right)}, \quad (9)$$

and k_{max} is given by the largest wavenumber of the Alfvén waves, which is fixed by the condition that the frequency of the waves cannot exceed the proton cyclotron frequency, namely $\omega < \Omega_p$. It follows that $k_{max} \sim \Omega_p / v_A$ (in the following, for consistency with Paper I, we take $k_{max} \sim \Omega_p / v_M$, v_M being the magnetosonic velocity).

3 EQUATIONS AND COUPLING

3.1 Time Evolution of Particles and Waves

In this Section we summarize the formalism that we introduced in Paper I for the description of the time-dependent interaction between the particles and the waves. The evolution of the electron (and positron) number density is given by the diffusion equation, which includes energy losses and gains (Paper I and references therein):

$$\frac{\partial N_e(p, t)}{\partial t} = \frac{\partial}{\partial p} \left[N_e(p, t) \left(\left| \frac{dp}{dt} \right|_{\text{rad}} + \left| \frac{dp}{dt} \right|_i - \frac{1}{p^2} \frac{\partial}{\partial p} (p^2 D_{pp}) \right) \right] + \frac{\partial^2}{\partial p^2} [D_{pp} N_e(p, t)] + Q_e[p, t; N_p(p, t)]. \quad (10)$$

Here $Q_e[p, t; N_p(p, t)]$ represents the injection rate of secondary relativistic electrons and positrons generated during the collisions between the accelerated relativistic protons with the thermal protons in the ICM (Sect. 3.3). A similar equation can be written for protons (Paper I and references therein) :

$$\frac{\partial N_p(p, t)}{\partial t} = \frac{\partial}{\partial p} \left[N_p(p, t) \left(\left| \frac{dp}{dt} \right| - \frac{1}{p^2} \frac{\partial}{\partial p} (p^2 D_{pp}) \right) \right] + \frac{\partial^2}{\partial p^2} [D_{pp} N_p(p, t)]. \quad (11)$$

The evolution of the spectrum of the Alfvén waves is described through a diffusion equation in the wavenumber space (Eilek 1979):

$$\frac{\partial W_k(t)}{\partial t} = \frac{\partial}{\partial k} \left(D_{kk} \frac{\partial W_k(t)}{\partial k} \right) - \sum_{i=1}^n \Gamma^i(k) W_k(t)$$

$$+I_k(t), \quad (12)$$

where D_{kk} is the diffusion coefficient due to wave-wave coupling (Sect. 3.2.2), Γ is the damping rate of the Alfvén waves with particles (Sect. 3.2.1) and I_k is the injection rate of the Alfvén waves (Sect. 3.2.3). In Eq.(12) we use the assumption, commonly made, that wave-wave interaction is just local in the wave number space.

3.2 Damping Processes, wave-wave coupling and injection of turbulence

All the relevant processes related to wave-particle interactions, wave-wave interactions and injection of Alfvén waves in the ICM are described in detail in Paper I. Here we only provide the reader with a brief overview of the main processes that we include in our calculations.

3.2.1 Damping Processes

In the case of nearly parallel wave propagation (i.e., $k_\perp \ll m\Omega/p$, $k \simeq k_\parallel$) and isotropic distribution of the velocities of the particles, the cyclotron resonant damping rates for Alfvén waves with particles of species α are given by Melrose (1968):

$$\Gamma_k^\alpha(t) = -\frac{4\pi^3 e^2 v_A^2}{kc^2} \int_{p_{\min}}^{p_{\max}} p^2 (1 - \mu_\alpha^2) \frac{\partial f_\alpha(p, t)}{\partial p} dp = \frac{\pi^2 e^2 v_A^2}{kc^2} \int_{p_{\min}}^{p_{\max}} (1 - \mu_\alpha^2) \left(2 \frac{N_\alpha(p, t)}{p} - \frac{\partial N_\alpha(p, t)}{\partial p} \right) dp, \quad (13)$$

where, in the relativistic case one has :

$$\mu_\alpha^{\text{rel}} = \frac{v_A}{c} \pm \frac{\Omega_\alpha m_\alpha}{pk}. \quad (14)$$

and in the non relativistic case:

$$\mu_\alpha^{\text{th}} = \frac{v_A m_\alpha}{p} \pm \frac{\Omega_\alpha m_\alpha}{pk}. \quad (15)$$

The upper and lower signs in Eqs. 14-15 are for negative and positive charged particles respectively. Eq. 13 can also be used to evaluate the damping rate in the case of isotropic Alfvén waves with an approximation which is within a factor of ~ 3 (Lacombe 1977).

3.2.2 Wave-wave Cascade

Wave-wave interactions cause the spectrum of the waves to cascade, namely to broaden toward larger values of k . This is a diffusive process, with diffusion coefficient $D_{kk} = k^2/\tau_s$. The time τ_s is the spectral energy transfer time and can be written as $\tau_s \sim \tau_{NL}^2/\tau_3$ (Zhou & Matthaeus 1990), where $\tau_{NL} = \lambda/\delta v$ is the non-linear eddy-turnover time (δv is the rms velocity fluctuation at wavelength λ) and τ_3 is the time over which this fluctuation interacts with other fluctuations of similar size.

In the context of the Kolmogorov phenomenology, the Alfvén crossing time $\tau_A = \lambda/v_A$ exceeds τ_{NL} and the fluctuations of comparable size interact in one turnover time, namely $\tau_3 \sim \tau_{NL}$. Since the velocity fluctuation, δv , is related to the rms wave field, δB , by $\delta v^2/v_A^2 = \delta B^2/B^2$, the

diffusion coefficient can be written as (Miller & Roberts 1995):

$$D_{kk} \simeq v_A k^{7/2} \left(\frac{W_k(t)}{2W_B} \right)^{1/2}. \quad (16)$$

Given a spectrum of injection of waves per unit time, I_k , one simple possibility to estimate the cascade time scale is to use the spectrum of the waves in Eq. 16 as obtained from Eq. 12 under stationary conditions and without damping processes. In Paper I we found:

$$\tau_s = \frac{k^2}{D_{kk}} \sim \frac{1}{k} \left(\frac{B^2}{4\pi} \right)^{1/3} \left(v_A^2 I_k \right)^{-1/3}. \quad (17)$$

3.2.3 Injection of Alfvén waves in the ICM: the Lighthill mechanism

While the physics involved in the process of energy transfer between waves and particles for a given spectrum of waves is relatively well understood, the transformation of the wave spectrum starting from some injection at large scales is rather poorly known. The waves are expected to couple with relativistic particles when the turbulence has been enriched of short wavelength modes, so that the cascading is implicitly required to be rather efficient if the injection occurs on macroscopic scales. If however this is the case, it was shown (Yan & Lazarian 2004 and refs. therein) that the Alfvén waves reach the high- k part of the spectrum with a highly anisotropic spectrum, and the efficiency of particle acceleration is likely to be therefore drastically reduced. From this follows that the acceleration process is favored in those scenarios in which the injection of Alfvén waves occurs on relatively small scales to start with. One injection process in which this condition is fulfilled is provided by the so-called *Lighthill* mechanism (Kato 1968; Eilek & Henriksen 1984), which can convert some fraction of the large scale fluid turbulence on the larger scales into Alfvén waves on smaller scales. Following Fujita et al. (2003) and Paper I, we assume in our calculation that fluid turbulence is injected on large scales, for instance excited by a merger event, and that the *Lighthill* mechanism couples the fluid turbulence with MHD turbulence on smaller scales. We made the assumption here that the spectrum of the fluid turbulence (not the MHD turbulence) is in the form of a power law

$$W_f(x_f) = W_f^o x_f^{-m}, \quad (18)$$

in the range $x_o < x_f < x_f^{\max}$, where x_o is the wavenumber corresponding to the maximum scale of injection of the turbulence; we thus do not consider the possibility that turbulence may be injected simultaneously at many scales (e.g., Tsytoich 1972). The maximum wavenumber is where the effect of fluid viscosity starts to be important and it is of the order of $x_f^{\max} \sim x_o(\mathcal{R})^{3/4}$ (Landau & Lifshitz, 1959), \mathcal{R} being the Reynolds' number. Thus for high values of the Reynolds number in the ICM (and in a magnetized medium) the turbulence cascading can be an efficient process down to scales much smaller than kpc (Fujita et al. 2003; Paper I).

In the *Lighthill* process a fluid eddy may be thought of as radiating Alfvén waves at a wavenumber $k = (v_f(x)/v_A)x_f$. The Alfvén waves are expected to be driven only for $x_f > x_T$, x_T being the wavenumber at which the transition from large-scale ordered turbulence to small-scale

disordered turbulence occurs. This transition is usually assumed to take place at the Taylor scale (Eilek & Henriksen 1984), $l_T \sim l_o(15/\mathcal{R})^{1/2}$, where the Reynolds number is given by $\mathcal{R} = l_o v_f / \nu_K$, and ν_K is the kinetic viscosity.

The fraction of the fluid turbulence radiated in the form of MHD modes is small for all but the larger eddies, near the Taylor scale. Therefore the *Lighthill* radiation may be expected to not disrupt the fluid spectrum. The rate of radiation *via* the *Lighthill* mechanism into Alfvén waves of wavenumber k is (Eilek & Henriksen 1984; Fujita et al. 2003; Paper I):

$$I_k \simeq 2 \left| \frac{3-2m}{3-m} \right| \rho v_A^3 \left(\frac{v_f^2}{v_A^2 R} \right)^{\frac{3}{3-m}} \times k^{-3 \frac{m-1}{3-m}}, \quad (19)$$

where $\rho \sim \mathcal{E}_t / v_f^2$, with \mathcal{E}_t the energy density of the fluid turbulence, and

$$R = \frac{x_o W_f(x_o)}{x_T W_f(x_T)}. \quad (20)$$

3.3 Secondary Electrons

As discussed above, the main new ingredient added in this paper, compared with the calculations presented in Paper I is the presence of secondary electrons (and positrons), as generated in the hadronic inelastic interactions of cosmic rays with the thermal gas in the ICM. The decay chain that we consider is (Blasi & Colafrancesco 1999):

$$p + p \rightarrow \pi^0 + \pi^+ + \pi^- + \text{anything}$$

$$\pi^0 \rightarrow \gamma\gamma$$

$$\pi^\pm \rightarrow \mu + \nu_\mu \quad \mu^\pm \rightarrow e^\pm \nu_e \nu_\mu.$$

The spectrum of secondary electrons and positrons with energy E_e is given by the convolution of the spectra of protons, $N(E_p)$, with the spectrum of pions produced in a single cosmic ray interaction at energy E_p , ($F_\pi(E_\pi, E_p)$) and with the distribution of leptons from the pion decay, $F_e^\pm(E_e, E_\pi)$, (e.g., Moskalenko & Strong, 1998):

$$Q_e^\pm[p, t; N_p] = n_{th}^p c \int_{E_{tr}} dE_p \beta_p N(E_p) \sigma_\pi^\pm(E_p) \int dE_\pi F_\pi(E_\pi, E_p) F_e^\pm(E_e, E_\pi), \quad (21)$$

where $\sigma^\pm(E_p)$ is the inclusive cross section for pion production, E_{tr} is the threshold energy for the process to occur and the distribution of electrons and positrons is given by :

$$F_e^\pm(E_e, E_{\pi^\pm}) = \int dE_\mu F_e^\pm(E_e, E_\mu, E_\pi), \quad (22)$$

where $F_e^\pm(E_e, E_\mu, E_\pi)$ is the spectrum of electrons/positrons from the decay of a muon of energy E_μ produced in the decay of a pion with energy E_π .

At large values of E_p the differential cross section is sufficiently well described by the so-called Feynman scaling, with small deviations which can easily be taken into account. In the low energy part, when the reaction occurs close to the threshold, and in general at laboratory energies smaller

than ~ 10 GeV, the experimental data on pion production are rather poor, and the scaling behaviour is violated. Since in this paper we are going to calculate the spectrum of the reaccelerated secondary electrons and positrons, we are forced to use a source term which correctly describes the spectrum of the injected leptons over a broad energy range ($\gamma \sim 10^2 - 10^5$). A practical and useful approach to both the high energy and low energy regimes was proposed in Dermer (1986a) and reviewed by Moskalenko & Strong (1998), and is based on the combination of the isobaric model (Stecker 1970) and scaling model (Badhwar et al., 1977; Stephens & Badhwar 1981). Here we briefly describe the formalism and approximations used in our calculations and provide the main equations.

In the Stecker's model the pion production due to pp collisions near threshold is mediated by the excitation of the $\Delta_{3/2}$ isobar, which subsequently decays into a nucleon and a pion. In this case the spectrum of pions produced in a single cosmic ray interaction is given by (e.g., Dermer 1986a; Strong & Moskalenko 1998):

$$F_\pi(E_\pi, E_p) = \Gamma \int_{m_p c^2 + m_\pi c^2}^{\sqrt{s} - m_p c^2} \frac{dm_\Delta c^2 f_\pi(E_\pi, E_p; m_\Delta)}{(m_\Delta c^2 - m_\Delta^o c^2)^2 + \Gamma^2} \times \left(\tan^{-1} \left(\frac{\sqrt{s} - m_p c^2 - m_\Delta^o c^2}{\Gamma} \right) - \tan^{-1} \left(\frac{m_p c^2 + m_\pi c^2 - m_\Delta^o c^2}{\Gamma} \right) \right)^{-1}, \quad (23)$$

where $\Gamma \simeq 0.0575$ GeV is the width of the Breit-Wigner distribution, $m_\Delta^o c^2 \simeq 1.232$ GeV is the average rest energy of the Δ -isobar, and $s = 2m_p c^2 (E_p + m_p c^2)$ is the square of the energy in the center of mass frame,

$$f_\pi(E_\pi, E_p; m_\Delta) = \frac{1}{4m_\pi c^2 \gamma_\pi' \beta_\pi'} \left(\frac{H^+}{\beta_\Delta^+ \gamma_\Delta^+} + \frac{H^-}{\beta_\Delta^- \gamma_\Delta^-} \right), \quad (24)$$

where $H^\pm = 1$ for $\gamma_\Delta^\pm \gamma_\pi' (1 - \beta_\Delta^\pm \beta_\pi') \leq \gamma_\pi \leq \gamma_\pi' (1 + \beta_\Delta^\pm \beta_\pi')$ and $H^\pm = 0$ otherwise,

$$\gamma_\Delta^\pm = \gamma_c \gamma_\Delta^* (1 \pm \beta_c \beta_\Delta^*), \quad (25)$$

with

$$\gamma_\Delta^* = \frac{s + m_\Delta^2 c^4 - m_p^2 c^4}{2\sqrt{s} m_\Delta c^2} \quad (26)$$

the Lorentz factor of the Δ -isobar in the center of mass frame, and

$$\gamma_c = \sqrt{s} / 2m_p c^2 \quad (27)$$

is the Lorentz factor of the center of mass. Finally,

$$\gamma_\pi' = \frac{m_\Delta^2 + m_\pi^2 - m_p^2}{2m_\Delta m_\pi} \quad (28)$$

is the Lorentz factor of the pion in the Δ -isobar system.

At high energies the spectrum of pions can be approximated by the simple formula proposed by Berezhinsky & Kudryavtsev (1990):

$$F_\pi(E_\pi, E_p) = \frac{1}{2} \left[c_1 \left(1 - \frac{E_\pi}{E_p} \right)^{3.5} + c_2 \exp(-18 \frac{E_\pi}{E_p}) \right], \quad (29)$$

where $c_1 = 1.22$ and $c_2 = 0.92$. Thus the injection rate of pions is given by :

$$Q_\pi(E_{\pi^\pm}, t) = n_{\text{thr}}^p c \int_{p_{\text{thr}}} dp N_p(p, t) \beta_p \frac{F_\pi(E_\pi, E_p) \sigma^\pm(p_p)}{\sqrt{1 + (m_p c/p_p)^2}}, \quad (30)$$

and the injection rate of relativistic electrons/positrons is given by :

$$Q_{e^\pm}(p, t) = \int_{E_\pi} Q_\pi(E_{\pi^\pm}, t) dE_\pi \int dE_\mu F_{e^\pm}(E_\pi, E_\mu, E_e) F_\mu(E_\mu, E_\pi), \quad (31)$$

where, following Moskalenko & Strong (1998), in the calculation of the pion injection rate we combine the isobaric model (Eqs.23–24) with the scaling model (Eq. 29) and adopt a linear interpolation between the two regimes, in the energy range 3–7 GeV. In our calculations we adopt the fits to the inclusive cross section $\sigma^\pm(E_p)$ given in Dermer (1986b) which allow to describe separately the rates of generation of π^+ and π^- .

The pion decay is well known to generate a muon spectrum in the following form:

$$F_\mu(E_\mu, E_\pi) = \frac{m_\pi^2}{m_\pi^2 - m_\mu^2} \frac{1}{p_\pi}. \quad (32)$$

Muons are produced in a relatively narrow range of energies, between a kinematic minimum and maximum given by

$$E_{\mu, \text{min}} = \frac{E_\pi}{2m_\pi^2} (m_\pi^2(1 - \beta_\pi) + m_\mu^2(1 + \beta_\pi)), \quad (33)$$

and

$$E_{\mu, \text{max}} = \frac{E_\pi}{2m_\pi^2} (m_\pi^2(1 + \beta_\pi) + m_\mu^2(1 - \beta_\pi)). \quad (34)$$

In order to speed up the computation, we assume that the spectrum of muons is a delta-function at the energy $E_\mu = 1/2(E_{\mu, \text{min}} + E_{\mu, \text{max}})$. Therefore:

$$F_\mu(E_\mu, E_\pi) = \delta\left(E_\mu - E_\pi \frac{m_\pi^2 + m_\mu^2}{2m_\pi^2}\right). \quad (35)$$

The spectrum of electrons and positrons from the muon decay, $F_{e^\pm}(E_\pi, E_\mu, E_e)$, was calculated by Blasi & Colafrancesco (1999). Combining their results with Eqs. (31) and (35), we obtain the rate of production of secondary electrons/positrons :

$$Q_{e^\pm}(p, t) = \frac{8m_\pi^2 c}{m_\pi^2 + m_\mu^2} \int_{E_{\text{min}}(E_e)} dE_\pi \frac{Q_{\pi^\pm}(E_\pi, t)}{E_\pi \beta_\pi} F_e(E_e, E_\pi), \quad (36)$$

where $E_{\text{min}} = 2E_e m_\pi^2 / (m_\pi^2 + m_\mu^2)$, and

$$F_e(E_e, E_\pi) = \frac{5}{12} - \frac{3}{4}\lambda_\pi^2 + \frac{1}{3}\lambda_\pi^3 - \frac{P_\pi}{2\beta_\pi} \left(\frac{1}{6} - (\beta_\pi + \frac{1}{2})\lambda_\pi^2 + (\beta_\pi + \frac{1}{3})\lambda_\pi^3 \right),$$

$$\text{for } \frac{\gamma_\pi}{c}(1 + \beta_\pi)^2 > \frac{m_\pi^2 + m_\mu^2}{2m_\pi E_e};$$

and

$$= \frac{\lambda_\pi^2 \beta_\pi}{(1 - \beta_\pi)^2} \left[3 - \frac{2}{3}\lambda_\pi \left(\frac{3 + \beta_\pi^2}{1 - \beta_\pi} \right) \right] - \frac{P_\pi}{1 - \beta_\pi} \left\{ \lambda_\pi^2 (1 + \beta_\pi) - \frac{2\lambda_\pi^2}{1 - \beta_\pi} \left[\frac{1}{2} + \lambda_\pi (1 + \beta_\pi) \right] + \frac{2\lambda_\pi^3 (3 + \beta_\pi^2)}{3(1 - \beta_\pi)^2} \right\},$$

$$\text{for } \frac{\gamma_\pi}{c}(1 + \beta_\pi)^2 \leq \frac{m_\pi^2 + m_\mu^2}{2m_\pi E_e}.$$

Here $\lambda_\pi = 2m_\pi^2 E_e / (m_\pi^2 + m_\mu^2) E_\pi$, and we put

$$P_\pi = -\frac{1}{\beta_\pi} \frac{m_\pi^4}{m_\pi^4 - m_\mu^4} \left\{ 4 - \left[1 + \left(\frac{m_\mu}{m_\pi} \right)^2 \right]^2 \right\}. \quad (37)$$

Eqs.(36–37) are then combined with Eq. 10 to calculate the time evolution of the spectrum of the accelerated secondary leptons.

Finally, it is useful to derive the injection rate of secondary electrons/positrons at high energies (in the scaling approximation) and for a simple power law spectrum of cosmic ray protons, $N(E_p) = K_p E_p^{-s}$. In this case the inclusive cross section for the production of π^\pm is approximately that of π^0 and thus from Eqs.(36–37), one finds :

$$Q_{e^\pm}(p) = A(s) n_{\text{th}} K_p E_e^{-s} \left\{ \mathcal{P}_1 + \mathcal{P}_2 \ln\left(\frac{a E_e}{6.4 \text{ GeV}}\right) + \mathcal{P}_3 \left(\frac{a E_e}{\text{GeV}}\right)^{\frac{1}{2}} \right\} \quad (38)$$

where $A(s) = 64 \times c \times 10^{-27} a^{1-s}$, and we put

$$a = \frac{2m_\pi^2}{m_\pi^2 + m_\mu^2} \quad (39)$$

and

$$\mathcal{P}_1 = \left(\frac{\tilde{a}}{s^2} + \frac{\tilde{b}}{(s+2)^2} + \frac{\tilde{c}}{(s+3)^2} \right) \mathcal{I}_0 - \left(\frac{\tilde{a}}{s} + \frac{\tilde{b}}{s+2} + \frac{\tilde{c}}{s+3} \right) \mathcal{I}_1 \quad (40)$$

$$\mathcal{P}_2 = \left(\frac{\tilde{a}}{s} + \frac{\tilde{b}}{s+2} + \frac{\tilde{c}}{s+3} \right) \mathcal{I}_0 \quad (41)$$

$$\mathcal{P}_3 = 1.5 \times \left(\frac{\tilde{a}}{s+1/2} + \frac{\tilde{b}}{s+5/2} + \frac{\tilde{c}}{s+7/2} \right) \mathcal{I}_2 \quad (42)$$

where

$$\tilde{a} = \frac{5}{12} \left(1 + \frac{1}{5}(a^2 - 1) \frac{1 + (m_\mu/m_\pi)^2}{1 - (m_\mu/m_\pi)^2} \right) \quad (43)$$

$$\tilde{b} = -\frac{3}{4} \left(1 + (a^2 - 1) \frac{1 + (m_\mu/m_\pi)^2}{1 - (m_\mu/m_\pi)^2} \right) \quad (44)$$

$$\tilde{c} = \frac{1}{3} \left(1 + 2(a^2 - 1) \frac{1 + (m_\mu/m_\pi)^2}{1 - (m_\mu/m_\pi)^2} \right) \quad (45)$$

and where the integrals^{*} are defined as:

$$\mathcal{I}_0 = \int_0^1 \frac{dx}{x^{2-s}} \left[c_1 (1-x)^{\frac{7}{2}} + c_2 \exp(-18x) \right], \quad (46)$$

$$\mathcal{I}_1 = \int_0^1 \frac{dx \ln(x)}{x^{2-s}} \left[c_1 (1-x)^{\frac{7}{2}} + c_2 \exp(-18x) \right], \quad (47)$$

and

$$\mathcal{I}_2 = \int_0^1 \frac{dx}{x^{3/2-s}} \left[c_1 (1-x)^{\frac{7}{2}} + c_2 \exp(-18x) \right], \quad (48)$$

It follows that the slope of the spectrum of secondary electrons and positrons is essentially that of the cosmic ray protons in this approximation (e.g., Dermer 1986a; Blasi & Colafrancesco 1999). In addition, Eq. 38 describes the slight

* $\mathcal{P}_1=0.069, 0.046, 0.031, 0.022, \mathcal{P}_2=0.019, 0.013, 0.01, 0.007,$ and $\mathcal{P}_3=0.006, 0.004, 0.0033, 0.0025,$ in the case $s=2.0, 2.1, 2.2,$ and $2.3,$ respectively

departure from the simple power law shape which is due to the increase of the inclusive cross section with the energy of the scattering protons (e.g., Dermer 1986b).

As shown in Paper I, the spectra of protons as affected by the reacceleration are usually not power laws. Therefore the expressions given here for the case of power law spectra are in general not applicable, although in the following we will sometimes use them, where specified, in order to estimate orders of magnitude.

4 NUMERICAL CALCULATION OF THE SPECTRA OF PARTICLES AND WAVES

4.1 Basic Assumptions

A detailed modelling of the injection of MHD turbulence in galaxy clusters and of all the related processes of wave-particle coupling is a very complex matter and well above the capabilities of present numerical simulations and semi-analytical treatments. On the other hand, the basics of this process can be hopefully understood by making use of viable assumptions and simplifications: this is the aim of Sect.4–5.

We assume that the injection of turbulence starts in coincidence with a merger event and remains constant for the duration of such an event. As a necessary simplification the spectrum of fluid turbulence is taken in the form of a power law (Eq.18), which basically means that there is roughly a single driving scale. The turbulence that is injected is only fluid turbulence, while the MHD turbulence is developed later as a consequence of the *Lighthill* mechanism. We assume that the physical conditions in the ICM (namely magnetic field strength, temperature and number density of the thermal particles) do not change significantly during the time in which the turbulence is injected.

We also assume that there is no spatial diffusion of the particles during the period of injection of the fluid turbulence, and ignore the effect of the mixing processes which may take place during cluster merger events.

In addition we assume that the fluid turbulence and the MHD turbulence are isotropic and that the magnetic field is tangled enough to ensure that also the distribution of the accelerated particles is isotropic in pitch angle.

With these assumptions the interaction between waves and particles can be investigated by solving the set of coupled differential equations Eqs. 10, 11, and 12. We consider situations in which the amount of energy injected in the form of turbulence is typically much smaller than the thermal energy of the ICM, and thus the thermal distributions of electrons and protons are treated as stationary. Since the time scale of damping and cascading are much shorter than the particle acceleration time scale, following Paper I we adopt a *quasi stationary approach*, in which it is assumed that within each time-step the spectrum of the waves approaches a stationary solution (obtained by solving Eq. 12 with $\partial W/\partial t = 0$) and that this solution changes with time due to the evolution of the spectrum of the accelerated electrons and protons.

4.2 The wave-proton Boiler

As discussed in Paper I, Alfvén waves channel most of the energy into relativistic protons, therefore subtracting it from the electron component which is on the other hand responsible for the observed radiations. It follows that if protons are too abundant in the ICM, the MHD turbulence is too efficiently damped and the acceleration of electrons is suppressed. This process is in fact quite complex, since it depends on the non linear time-dependent interplay among the spectra of protons, electrons and waves.

The aim of this Section is uniquely to draw a few general conclusions on the efficiency of electron and positron acceleration in the ICM. To achieve this goal, we simply assume that the injection rate of Alfvén waves can be written as a power law, $I(k) = I_o k^{-\omega}$, and that, for simplicity, the spectrum of relativistic protons can also be approximated as a power law, $N_p(p) \propto p^{-s}$. Neither one of these assumptions is adopted in the detailed calculations that follow.

Within the context imposed by these simple assumptions, the efficiency of lepton acceleration can be estimated analytically. In particular, if τ_s is the time for spectral energy transfer due to wave-cascading and τ_d is the damping time of waves on the relativistic particles, one has two relevant asymptotic cases:

i) For $\tau_s \ll \tau_d$, the spectrum of the waves is driven by the injection of Alfvén waves and the process of wave-cascading. For roughly stationary regime, the spectrum of the waves can be estimated from Eqs.(12 and 16), and we can write:

$$W_k = (n_{th} m_p)^{\frac{1}{3}} \left(\frac{3}{5} \frac{I_{k_o} \times k_o}{\omega - 1} \right)^{2/3} k^{-\frac{5}{3}}. \quad (49)$$

The lepton diffusion coefficient in momentum space is obtained by combining Eq. 8 and Eq. 49:

$$D_{pp} \propto \left(\frac{I_o}{n_{th}} \right)^{\frac{2}{3}} B^{1/3}. \quad (50)$$

The efficiency of electron and positron acceleration increases when I_o/n_{th} increases and it slightly increases with increasing B . Thus, if the turbulence is smoothly injected in the cluster volume with an injection rate which scales with the thermal energy density, the efficiency of lepton acceleration is expected to be slightly higher in the high field regions. On the other hand, if the injection rate of the turbulence does not depend on the local energy density of the thermal ICM, then electrons are accelerated with higher efficiency in the low density regions.

ii) For $\tau_s \gg \tau_d$, the spectrum of the waves is determined by the injection of Alfvén waves and their damping, which is mainly caused by resonant scattering with relativistic protons. From Eq. 12 and from the damping rate due to relativistic protons (Eq. 58 in Paper I) one has:

$$W_k = \frac{c}{2\pi^2 v_A^2} \left(\frac{p_{low}/(m_p c)}{e m_p} \right)^{2-s} \frac{B^s I_o s}{\mathcal{E}_p s - 2} k^{1-(\omega+s)}. \quad (51)$$

The diffusion coefficient in momentum space for electrons and positrons can therefore be obtained by combining Eq. 8 and Eq. 51:

$$D_{pp} \propto \frac{I_o}{\mathcal{E}_p} B^{1-\omega}. \quad (52)$$

It follows that the efficiency for lepton acceleration increases

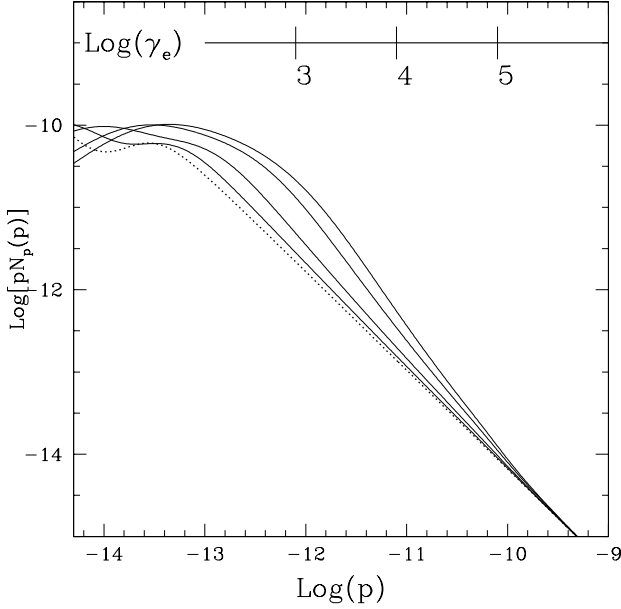


Figure 1. Time evolution of the proton spectrum. From bottom to top, we plot the spectra for $t = 0$ (dotted line), 10^{15} , 3×10^{15} , 7×10^{15} , and 10^{16} seconds after the start of the acceleration phase. The calculations are carried out assuming $n_{th} = 1.8 \times 10^{-3} \text{ cm}^{-3}$, $T = 10^8 \text{ K}$, $B(r = 0) = 1.4 \mu\text{G}$, $d/dt(\delta B)^2/8\pi = 1.2 \times 10^{-28} \text{ erg cm}^{-3} \text{ s}^{-1}$, and $\mathcal{E}_p = 10^{-2} \mathcal{E}_{th}$ (with $s = 2.2$). In the Figure we also show the axis with the values of the Lorentz factors of the secondary electrons and positrons produced by the corresponding cosmic ray protons.

with increasing I_o/\mathcal{E}_p and with decreasing B (at least for $\omega > 1$).

In general, the damping of waves due to resonant scattering with protons and the process of cascading of waves contribute roughly equally to the modification of the spectrum of the Alfvén waves in the ICM, so that a *realistic* situation can be thought of as intermediate between the two regimes discussed above, at least at the beginning of the reacceleration phase.

On the other hand, when reacceleration has started, energy is transferred from waves to protons, and the damping due to this process is expected to increase with time. This effect is more pronounced where the Alfvén velocity is larger. As shown in Paper I, a general feature of the reacceleration picture in the presence of hadrons is that the acceleration efficiency is slightly higher in the low density regions so that the radio emission due to the synchrotron radiation of electrons may have a very broad profile as a function of the radial distance from the cluster center.

4.3 The spectrum of relativistic protons

Due to the confinement phenomenon and the negligible energy losses of hadrons in the ICM, the spectrum of the protons after the reacceleration phase is left basically unchanged.

In Fig. 1 we illustrate an example of the time evolution of the spectrum of protons assuming physical conditions typical of the core of a massive cluster. We confirm the finding

of Paper I, in which we showed that the spectrum of relativistic protons may be substantially modified in the energy range 1 GeV - 100 GeV due to the resonant interaction with MHD Alfvénic turbulence. This is a consequence of the fact that the acceleration time for protons is minimum at these energies (see Fig. 16 in Paper I). Indeed, at smaller scales (which resonate with smaller values of the proton energy) $\tau_s \gg \tau_d$ and the acceleration time should decrease with particle's momentum as (from Eqs. 8-9 & 51):

$$\tau_{\text{acc}}(p) = p^3 / \frac{\partial(p^2 D_{pp})}{\partial p} \propto \frac{p^2}{D_{pp}} \propto p^{-(\omega+s)+3}, \quad (53)$$

while at larger scales (which resonate with more energetic protons) $\tau_s \ll \tau_d$ and the acceleration time should increase with the momentum of the particles (from Eqs. 8-9 & 49) as:

$$\tau_{\text{acc}}(p) \propto p^{1/3}. \quad (54)$$

In Fig. 1 we also mark the typical regions of the spectrum of the hadrons which approximatively contribute to the injection of the secondary electrons and positrons with a given Lorentz factor. The consequence of the decrease of the efficiency of Alfvén acceleration with increasing proton energy is that only the amount of secondary electrons/positrons injected at $\gamma \sim 10^2 - 10^3$ is expected to be significantly increased. On the other hand, the injection rate of secondary electrons and positrons with $\gamma \sim 10^4$, which emit the synchrotron radiation at 0.3-1.4 GHz, is not expected to be substantially modified (at least not more than a factor of 2-3) by the Alfvén acceleration process.

4.4 Reacceleration of secondary electrons and positrons

The main point of this paper is to include the effect of the reacceleration of the secondary electrons and positrons, as generated in hadronic interactions of a time-dependent spectrum of protons. This phenomenon has a twofold effect on the observable non thermal radiation from a cluster: first, the secondary electrons and positrons add to the pool of (primary) electrons that can suffer the re-energization due to coupling with waves. Second, energy is channelled from waves to protons, therefore causing an increase with time of the relative weight of secondary electrons and positrons with respect to relic electrons.

The evolution of the spectra of particles (protons and electrons) and Alfvén waves is obtained by solving numerically Eqs. 10, 11, and 12 with $Q_e(p_e, t)$ given by Eq. 36. The spectrum of the secondary electrons and positrons at the beginning of the acceleration period is computed from the Fokker-Planck equation (Eq. 10, with the source term given by Eq. 36) under stationary conditions and assuming $D_{pp} = 0$ (e.g., Dolag & Ensslin 2000):

$$N_e(p) = \frac{1}{\left| \left(\frac{dp}{dt} \right)_{\text{rad}} + \left(\frac{dp}{dt} \right)_i \right|} \int_p^{p_{\text{max}}} Q_e(p) dp. \quad (55)$$

Our general findings, illustrated in Fig. 2, are summarized below.

As in the case of the reacceleration of relic primary electrons (Paper I), the efficiency for lepton acceleration decreases with increasing energy of relativistic hadrons in

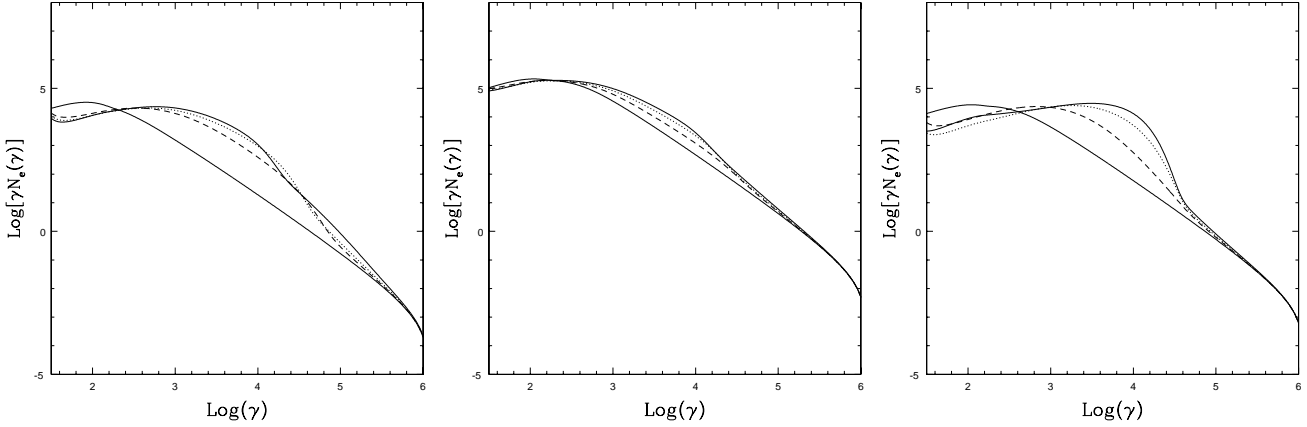


Figure 2. Time evolution of the spectra of leptons. The spectra are given at $t = 0$ (thick solid lines), 3×10^{15} (dashed lines), 7×10^{15} (dotted lines), and 1.2×10^{16} seconds (solid lines) after the start of the acceleration phase. **Panel a):** calculations are performed assuming $n_{th} = 2 \times 10^{-4} \text{ cm}^{-3}$ and $\mathcal{E}_p = 8\%$ of the thermal energy density. **Panel b):** calculations are performed assuming $n_{th} = 10^{-3} \text{ cm}^{-3}$ and $\mathcal{E}_p = 8\%$ of the thermal energy density. **Panel c):** calculations are performed assuming $n_{th} = 10^{-3} \text{ cm}^{-3}$ and $\mathcal{E}_p = 1\%$ of the thermal energy density. For all the panels the other parameters are $s = 2.2$, $T = 10^8 \text{ K}$, $B(r = 0) = 0.5 \mu\text{G}$ and $d/dt(\delta B)^2/8\pi = 1.3 \times 10^{-28} \text{ erg cm}^{-3} \text{ s}^{-1}$.

the ICM. As a consequence, the prominence of the bump of accelerated particles that appears in Fig. 2 is expected to decrease when the energy content in the form of hadrons increases.

A pronounced feature appears in the spectrum of leptons, due to the reacceleration process, namely a sharp drop in the spectrum, followed by a flattening. The drop can be easily understood in terms of balance between energy losses of relativistic leptons and rate of re-energization due to resonant interaction with waves. The flattening is simply due to the secondary electrons and positrons continuously generated in the hadronic interactions of cosmic rays in the ICM. Once the reacceleration period becomes longer than the acceleration time-scale, the typical energy at which this feature appears tends to decrease with time, as a consequence of the enhanced damping of the waves on the proton component. As a general comment, we point out that the presence of reacceleration boosts the number of leptons with $\gamma \sim 10^4$ by 1–2 orders of magnitude with respect to the case without reacceleration.

After the end of the reacceleration stage, the spectrum of protons remains basically unchanged. As a consequence, the spectrum of secondary electrons and positrons generated after the reacceleration is stopped is also time-independent, and determined only by the duration and by the efficiency of the reacceleration phase.

4.5 Reacceleration of Relic and secondary electrons: *Hybrid Models*

In Paper I we discussed at length the possibility of reaccelerating relic electrons, possibly injected within the cluster volume either at shocks, or in AGNs or ordinary galaxies. When these injection processes take place at redshift $z < 0.5$, electrons with Lorentz factor $\gamma \sim 200 - 500$ may have a lifetime of $\sim 10^9$ to 10^{10} yrs depending on whether they are injected in the center or in the outskirts of the cluster, respectively (Sarazin 1999; Brunetti 2003). It follows that, at least in the

external parts of a cluster there may be a sufficiently high abundance of relic electrons to be reaccelerated by the MHD turbulence.

In this Section we describe the result of the reacceleration of both components, namely relic electrons and secondary electrons and positrons. We name these scenarios *Hybrid Models*.

As in the previous Section the evolution of the spectra of particles (protons, electrons and positrons) and Alfvén waves is obtained by solving numerically Eqs. 10, 11, and 12 with $Q_e(p_e, t)$ given by Eq. 36. In this case, however, the initial spectrum of the electrons is the combination of the spectrum of the secondary electrons and positrons at the beginning of the acceleration period (Eq. 55) and of the spectrum of the relic–primary electrons accumulated in the ICM.

In Fig. 3 we plot the spectrum of the reaccelerated electrons and positrons as obtained in the cluster center and in the cluster outskirts (see the caption for the numerical values adopted there). In Fig. 3 we assume that the strength of the magnetic field in the cluster volume scales according with flux conservation ($B \propto n_{th}^{2/3}$) and that the injection power of Alfvén waves is $P_A = \int I_k dk \propto n_{th}^{5/6}$ (see Sect. 5.1 and Paper I). The number density of the relic (primary) electrons and of the relativistic hadrons in the cluster volume scales with that of the thermal particles. Assuming that the energy density of the relativistic protons is of the order of 10^{-2} times that of the thermal plasma, from Fig. 3 it follows that the reacceleration process of secondary electrons/positrons could be important. In particular, we find that a relevant contribution (from ~ 50 to 80%) to the spectrum of the radiating electrons and positrons with $\gamma \sim 10^3 - 10^4$ in the central regions of the cluster is provided by reaccelerated secondary electrons and positrons. On the other hand, the spectrum of electrons in the external regions is essentially contributed by the reaccelerated relic electrons. In the presence of processes that make the spatial distribution of relativistic protons broader than the thermal gas, we can expect

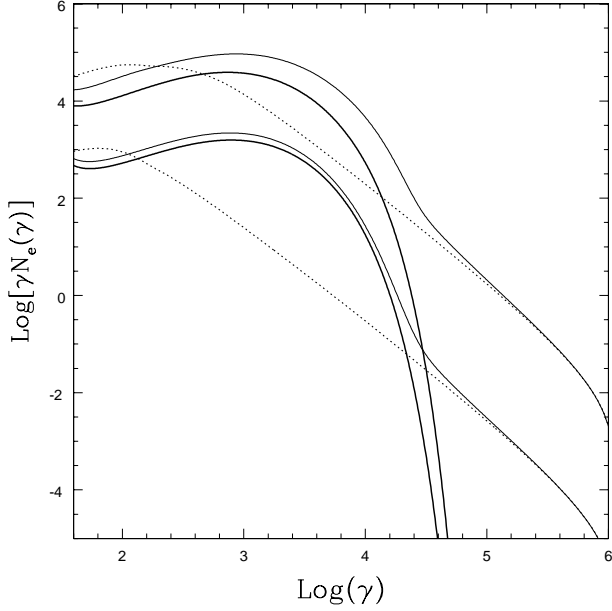


Figure 3. Spectra of accelerated electrons and positrons in a cluster core (upper curves) and in the cluster outskirts (lower curves) at $t = 7 \times 10^{15}$ s from the beginning of the acceleration phase. Calculations in the cluster core are performed assuming $n_{th} = 2 \times 10^{-3} \text{ cm}^{-3}$, $B(r=0) = 1.5 \mu\text{G}$, and $d/dt(\delta B)^2/8\pi = 1.19 \times 10^{-28} \text{ erg s}^{-1} \text{ cm}^{-3}$. In the cluster outskirts we assume $n_{th} = 7 \times 10^{-5} \text{ cm}^{-3}$, $B(r=0) = 0.16 \mu\text{G}$, and $d/dt(\delta B)^2/8\pi = 7.8 \times 10^{-30} \text{ erg s}^{-1} \text{ cm}^{-3}$. $\mathcal{E}_p = 1\%$ of the thermal energy density (with $s = 2.2$), $T = 10^8 \text{ K}$ are assumed in both the cluster core and outskirts. The thin solid curves are the total spectra derived from the reacceleration of a population of relic primary electrons with $\mathcal{E}_e = 10^{-5} \mathcal{E}_{th}$ mixed with the population of secondary electrons and positrons. The thick solid curves mark the contribution of the accelerated relic electrons only. For comparison, the stationary spectra of the secondary electrons and positrons in the ICM at the beginning of the acceleration are also given in both cases (dotted lines). The high energy cut-off in the spectrum of secondary particles is due to a high energy cut-off fixed at 10 TeV in the spectrum of protons.

that the contribution provided by the central denser regions of the cluster gets somewhat suppressed. At the same time, since in the cluster outskirts the Coulomb losses of the relativistic electrons are less efficient than in the cluster center, the radial distribution of the number density of relic electrons may be broader than that assumed in Fig. 3 and consequently their contribution to the total spectrum of the reaccelerated leptons may be even larger.

5 HYBRID MODELS: PHENOMENOLOGY OF NON THERMAL EMISSION FROM GALAXY CLUSTERS

Here we apply the formalism described in the previous Sections and calculate the expected non thermal emission from galaxy clusters, when both relic electrons and secondary electrons and positrons are present during the stage of injection of turbulence and resonant reacceleration.

5.1 Basic Assumptions

In this Section we briefly discuss the basic assumptions adopted for the calculations of particle acceleration and non-thermal emission from galaxy clusters. The assumptions are relative to the physical properties of the ICM and of the relativistic component, and to the modelling of the injection of turbulence in the cluster volume.

We assume a β -model (Cavaliere & Fusco-Femiano, 1976) for the radial density profile of the thermal gas in the ICM, in the form

$$n_{th}(r) = n_{th}(r=0) \left(1 + \left(\frac{r}{r_c}\right)^2\right)^{-3\beta/2}, \quad (56)$$

where r_c is the core radius and $\beta = 0.8$. The magnetic field is taken in its flux conserving form:

$$B(r) = B(r=0) \left(\frac{n_{th}(r)}{n_{th}(r=0)}\right)^{2/3}. \quad (57)$$

Here we explore the region of values $B(r=0) \sim 0.5\text{--}3 \mu\text{G}$, expected to reproduce the uncertainty in the value of the magnetic field as derived from different techniques.

Following Fujita et al.(2003) and paper I, we assume that large scale fluid turbulence is injected in the ICM during cluster mergers and that the turbulent eddies at small scales radiate MHD waves due to the *Lighthill* mechanism (Sect. 3.2.3).

For simplicity we assume that the maximum injection scale of the turbulence, the Reynolds number and the velocity of the turbulent eddies, which are essentially unknown quantities, are independent from the location within the cluster volume. Under these simplified conditions, in Paper I we showed that the injection power in the form of Alfvén waves scales as:

$$P_A(r) = \int I_k(r) dk = P_A(r=0) \left(\frac{n_{th}(r)}{n_{th}(r=0)}\right)^{5/6}. \quad (58)$$

Finally we assume that the spatial profile of the number density of the relic electrons and of the relativistic protons (at the beginning of the acceleration period) scales with that of the thermal matter:

$$\mathcal{E}_{p[e]} = \mathcal{E}_{th} \eta_{p[e]}, \quad (59)$$

where $\eta_{p[e]}$ is a parameter; a reference value, $s = 2.2$, is adopted for the injected spectrum of the cosmic ray protons. As a matter of fact the use of Eq.(59) limits ourselves to assume a fairly uniform distribution (non-patchy) of relativistic particles in the ICM. On the other hand, patches of relativistic plasma separated from the thermal pool are clearly detected by radio and X-ray observations (e.g., Fabian et al. 2000; McNamara et al., 2000) which show the presence of bubbles and cavities in a few galaxy clusters. However, it is expected that such bubbles will expand with time and mix in the ICM due to the developing of instabilities in a time scale of the order of a few 10^8 yrs (Churazov et al., 2000; Brüggén & Kaiser 2001) which is a short time scale with respect to the duration of the injection process of the bulk of cosmic rays in galaxy clusters. Thus the assumption of a fairly uniform mixing between thermal and relativistic plasma in galaxy clusters is justified for the aim of the present paper.

5.2 Particle acceleration in cluster cores

In this Section we focus on the synchrotron emission expected from the cores of galaxy clusters and derive constraints on the physical properties of the ICM. We focus on cluster cores since in these regions the larger gas density makes the pp interactions more frequent and therefore the density of secondary particles larger. Moreover the magnetic field is expected to be larger in the center. These two facts imply a larger synchrotron emissivity in these regions. On the other hand, if relativistic protons have more than a few percent of the local thermal energy density, the damping of waves becomes too large and the electron acceleration gets suppressed, therefore reducing the synchrotron emissivity. It follows that the general situation may be rather complex.

This complexity is illustrated in Fig. 4 where we plot the synchrotron emissivity as a function of the ratio of the energy densities in the relativistic protons and the thermal plasma at the beginning of the reacceleration stage, $\mathcal{E}_p/\mathcal{E}_{th}$, for different values of B and of P_A .

As expected, for small values of $\mathcal{E}_p/\mathcal{E}_{th}$ the damping rate is less efficient than the cascading process and the synchrotron emissivity simply scales with $\mathcal{E}_p/\mathcal{E}_{th}$ (Eq. 52); at this stage, for the adopted rates of turbulence-injection, the synchrotron emission is more than one order of magnitude larger than in the case without reacceleration. Increasing $\mathcal{E}_p/\mathcal{E}_{th}$, the damping of waves on protons increases and the acceleration efficiency decreases, so that the synchrotron emissivity is reduced as well. Fig. 3 also shows that when the ratio $\mathcal{E}_p/\mathcal{E}_{th}$ is larger than $\sim 10 - 20\%$, then the reacceleration of leptons with $\gamma \sim 10^4$ is basically stopped and the synchrotron emissivity approaches that expected from the standard secondary model.

When this saturation effect does not occur, the synchrotron emissivity in the central region may easily exceed the observations. As a result, such observations can be used to impose constraints on the physical conditions in which the reacceleration of secondary particles takes place. As usual we refer to the case of the Coma cluster as the case in which the observations are richer. The conclusions that we will draw below should not be extended to other clusters, until comparable wealth of data is obtained for those clusters.

The main observational constraints can be summarized as follows:

i) Radio brightness of the core region: we use the 327 MHz VLA profile obtained after the subtraction of point-like sources (Govoni et al. 2001). The allowed region of the brightness of the core region can be estimated by subtracting the contribution due to the external regions to the brightness integrated along the line of sight.

ii) Radio spectrum of the core region: the 327-1400 MHz spectral index map of the Coma radio halo shows a plateau in the central regions and a prominent radial steepening of the slope of the spectrum (Giovannini et al. 1993). The plateau region roughly coincides with the cluster core and the synchrotron spectrum there is slightly flatter than $\alpha \sim 0.9$.

iii) Radio brightness in the frequency range 2.7-5 GHz: At these high frequencies the radio emission imposes strong constraints on all flavors of secondary models, as discussed by Reimer et al. (2004).

In Fig. 4 we compare our theoretical expectations, as obtained for different values of the model parameters (P_A , B and $\mathcal{E}_p/\mathcal{E}_{th}$), with the constraints listed above.

The weakest limits are clearly those obtained for low values of the magnetic field. For $B = 1\mu G$ (left panel in Fig. 4), low rates of injection of waves select the region with values of $\mathcal{E}_p/\mathcal{E}_{th}$ larger than about 10^{-3} . On the other hand, as soon as the rate of injection increases above $\sim 8 \times 10^{-29} \text{ erg cm}^{-3} \text{ s}^{-1}$ (which implies a total energy budget injected per unit volume in the form of Alfvén waves $\sim 1.5\%$ of the thermal energy density), the allowed values of $\mathcal{E}_p/\mathcal{E}_{th}$ drop below a few 10^{-3} . The high frequency data of the Coma cluster impose an upper limit $\mathcal{E}_p/\mathcal{E}_{th} < 0.05$.

Assuming $B = 3\mu G$ (right panel in Fig. 4) it is clear that the observed synchrotron brightness excludes big chunks of the parameter space. In particular, assuming an appreciable injection rate of energy of Alfvén waves in the cluster core ($\geq 0.5\%$ of the thermal energy) it is found that intermediate values of the ratio $\mathcal{E}_p/\mathcal{E}_{th}$ are not allowed. The region $\mathcal{E}_p/\mathcal{E}_{th} > 10^{-2}$ is excluded by the high frequency points in the spectrum of the radio halo of the Coma cluster (arrows in Fig. 4).

The most difficult observational constraint to match is the combination of low synchrotron brightness *i)* and flat radio spectrum *ii)*. A relatively low value of the acceleration efficiency cannot reproduce a synchrotron spectrum as flat as the observed one. Therefore an efficient particle acceleration mechanism is requested to boost electrons toward higher energies and to flatten the emitted synchrotron spectrum. In order to avoid to exceed the observed brightness, a relatively small injection rate of secondary electrons and positrons is required. More quantitatively, we find that the parameter space with $\mathcal{E}_p/\mathcal{E}_{th} > 10^{-3}$ is excluded for this strongly magnetized case.

5.3 Integrated broad band spectrum

In this Section we illustrate our calculations of the volume integrated fluxes of radiation generated by reaccelerated electrons and positrons through synchrotron emission and IC. The central gas density, $n_{th}(r=0)$, the β parameter and the core radius r_c are chosen as the representative values of the Coma cluster (Briel et al. 1992).

In Fig. 5 we plot our results for the synchrotron spectra (left panel) and the IC spectra (right panel). The data points refer to the radio, hard X-ray and gamma ray bands. All curves are obtained in the assumption that the cosmic ray energy density at the beginning of the reacceleration stage is proportional to the thermal energy density at any point. The values of $P_A(r=0)$ and the ratio $\mathcal{E}_p/\mathcal{E}_{th}$ are not chosen to obtain a best fit to the data, they are only fixed in order to provide a viable representation of the data.

Some general remarks emerge from the inspection of Fig. 5 :

i) The synchrotron luminosity of a Coma-like radio halo can be easily matched even with $\mathcal{E}_p/\mathcal{E}_{th} \sim 10^{-3} - 10^{-2}$ and $\sim \mu G$ strengths of the central magnetic field. This energy requirement is more than one order of magnitude below that of classical secondary models (Blasi & Colafrancesco 1999; Dolag & Ensslin 2000).

ii) The steepening of the integrated synchrotron spectrum

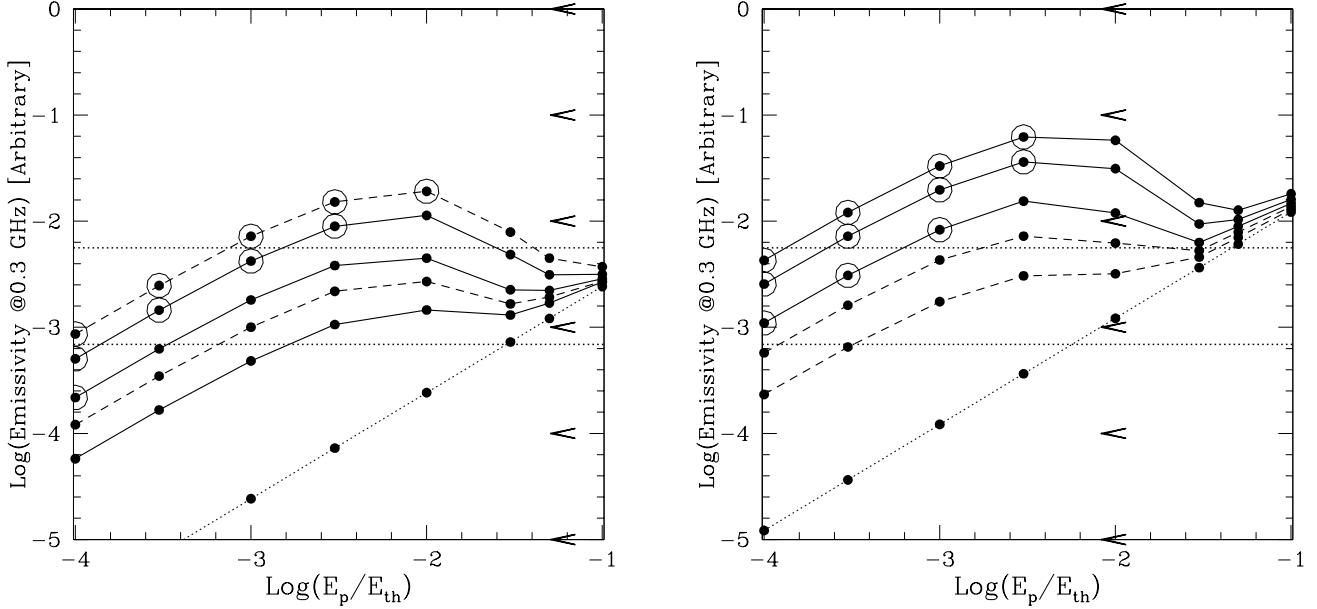


Figure 4. Synchrotron emissivity at 330 MHz (in arbitrary units) as a function of the ratio between cosmic rays and thermal energy densities at the beginning of the reacceleration stage ($\mathcal{E}_p/\mathcal{E}_{th}$) for the core region of the Coma cluster calculated after a reacceleration period $\Delta\tau_{acc} = 10^{16}$ s. The horizontal dotted lines give the upper and lower bounds of the allowed range of the synchrotron emissivity obtained from the observed brightness profile at 330 MHz (estimated from the deprojection of the observed profile given by Govoni et al. 2001). Arrows give the limits on the ratio $\mathcal{E}_p/\mathcal{E}_{th}$ obtained from the high frequency radio data (Reimer et al. 2004) and assuming that all the emission at these frequencies comes from the core region. Circles mark the points in the diagram for which the synchrotron spectral index is consistent with that observed (from Giovannini et al. 1993). **Panel a):** Calculations are carried out for $B(r=0) = 1\mu\text{G}$. The different curves refer to different assumed injection rates for Alfvén waves ($d/dt(\delta B)^2/8\pi$): 1.87, 1.3, 0.83, 0.64, and $0.47 \times 10^{-28} \text{erg s}^{-1} \text{cm}^{-3}$ (from top to bottom, respectively). **Panel b):** Calculations are carried out for $B(r=0) = 3\mu\text{G}$. The different curves refer to different assumed injection rates for Alfvén waves ($d/dt(\delta B)^2/8\pi$): 1.3, 0.83, 0.47, 0.33 and $0.21 \times 10^{-28} \text{erg s}^{-1} \text{cm}^{-3}$ (from top to bottom, respectively).

of the Coma radio halo can be reproduced only for cosmic ray energy density of the order of $\mathcal{E}_p \leq 5\%$ or lower. This is because a larger content of cosmic ray protons would decrease the efficiency of the lepton acceleration and reduce the synchrotron bump at lower frequencies.

iii) The observed hard X-ray spectra are hardly achievable if only the effect of reaccelerated secondary particles is taken into account. This is mainly due to the low number of secondaries generated if the energy density in the form of relativistic protons is the one inferred in our point *i*).

If the injection of waves takes place on a spatial scale which is appreciably broader than that in Eq. 58, the efficiency of the reacceleration of secondary particles increases in the external volume and the IC emission in the outskirts can be enhanced, leaving the synchrotron emission almost unaffected, due to the rapid decrease of the value of the magnetic field with radius. However, we find that a flux of HXR close to the observed one can be obtained only by assuming rather extreme conditions in the cluster outskirts (e.g., $\mathcal{E}_t \sim \mathcal{E}_{th}$). Furthermore we find that in this case the strong back-reaction of the accelerated protons would suppress the acceleration of electrons within $\sim 10^8$ yrs.

Similarly an appreciably larger IC luminosity cannot be produced if the spatial distribution of the cosmic ray protons is broader than that of the thermal plasma. Indeed, although in this case a larger number of secondary electrons and positrons is produced in the external volume, the

stronger back reaction of protons on the waves inhibits the acceleration of electrons/positrons in these regions.

iv) Due to the relatively poor efficiency of the reacceleration mechanism, Alfvén waves in the ICM cannot accelerate very high energy electrons (say $\gamma \geq 10^5$) and thus the energy distribution of the electrons and positrons which are responsible for the emission of gamma rays though IC is not appreciably affected by the reacceleration scenario discussed here. This is the reason why in the pure reacceleration models, with no protons and no secondary particles, we expect no gamma ray emission. The limit imposed on the energetic budget in the form of high energy protons from the EGRET upper limit (Reimer et al. 2004) is at the level of 20% of the thermal energy, obtained by assuming that the all gamma ray flux is generated through pion decays. For cosmic ray energy densities below this bound (but larger than a few times 10^{-3} of the thermal energy), an anti-correlation appears between the IC HXRs and the IC gamma rays (we recall that the latter are only generated by the secondary electrons and positrons); a similar anti-correlation is expected between the IC HXRs and the gamma rays generated by the decay of π^0 . A detailed analysis of the gamma ray emission expected from reacceleration models will be presented in a forthcoming paper (Brunetti et al., in prep.).

v) In principle the broad band non-thermal spectrum of the Coma radio halo can be reproduced if both relic elec-

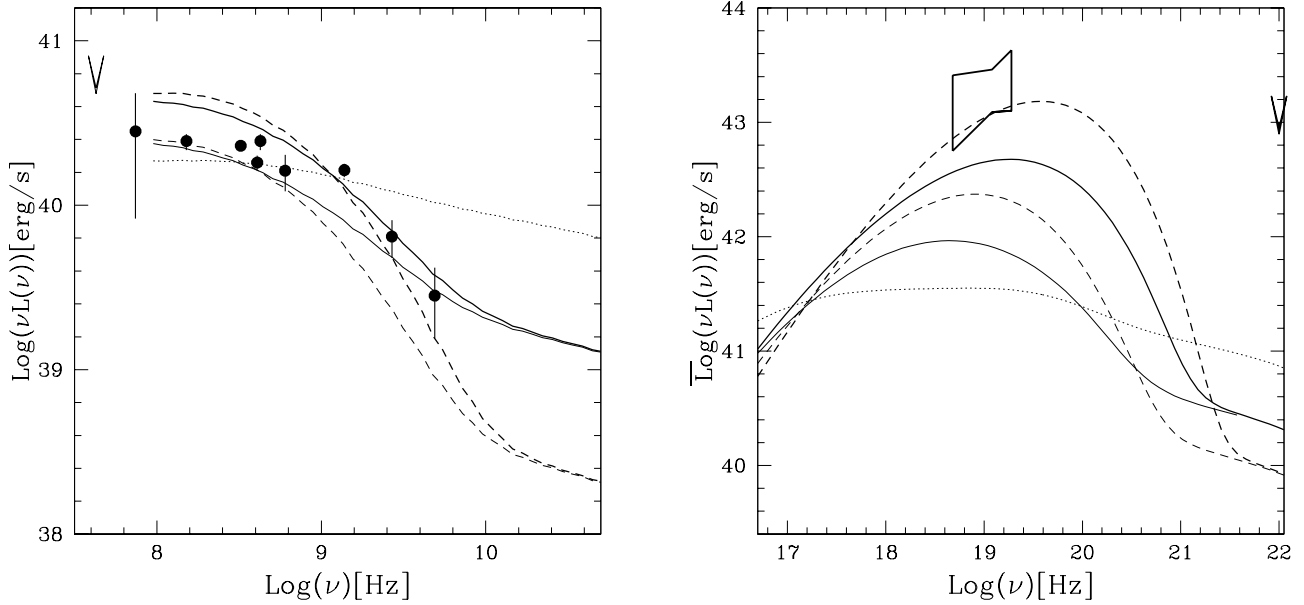


Figure 5. Expected synchrotron (left panel) and IC (right panel) spectra calculated for the Coma cluster. All the calculations are carried out assuming that the injection rate of Alfvén waves in the center of the cluster is $P_A(r=0) = 1.3 \times 10^{-28} \text{ erg s}^{-1} \text{ cm}^{-3}$ and for $\Delta t_{acc} = 10^{16}$ s. Calculations are carried out for both $P_A \propto n_{th}^{5/6}$ (Eq. 58) (thin lines) and $P_A \propto n_{th}^{1/2}$ (thick lines). The different models refer to the following cases: $B(r=0) = 2.0 \mu\text{G}$ and $\mathcal{E}_p/\mathcal{E}_{th} = 0.12$ with no relic primary electrons (dotted lines), $B(r=0) = 1.7 \mu\text{G}$ and $\mathcal{E}_p/\mathcal{E}_{th} = 0.03$ with no relic primary electrons (solid lines), and $B(r=0) = 1.1 \mu\text{G}$ and $\mathcal{E}_p/\mathcal{E}_{th} = 0.01$ with $\mathcal{E}_e/\mathcal{E}_{th} = 5 \times 10^{-5}$ independent of the distance from the center (dashed lines).

trons and secondary electrons/positrons are present[†]. If a few percent of the thermal energy are stored in the relativistic protons, the synchrotron spectrum may be dominated by the radiation from reaccelerated secondary electrons and positrons, mainly in the central regions of the cluster. At the same time, the IC emission is dominated by reaccelerated relic electrons in the external regions (i.e. at $2 < r/r_c < 5$).

Obviously the contribution of the reaccelerated secondary electrons and positrons to the integrated non-thermal spectrum of galaxy clusters is expected to fall down if the energy of cosmic ray protons is maintained well below $\sim 1\%$ of the thermal energy.

5.4 Radial profiles

The very broad extension of the synchrotron emission from giant radio halos is among the properties which are difficult to be fitted by secondary models (e.g., Brunetti 2004 and ref. therein). Although this Section is not devoted to a detailed comparison between observed synchrotron profiles and model expectations, here we show that Alfvénic reacceleration of secondary electrons and positrons in the ICM may generate relatively broad synchrotron profiles.

If the reacceleration period is much longer than the reacceleration time-scale, the bulk of the secondary electrons and positrons injected above the momentum, $p_>$, at which Coulomb losses outweigh the acceleration efficiency,

[†] For simplicity we assume Eq. 59 to hold also in the case of relic electrons.

is essentially boosted around a maximum momentum, p_{max} , at which acceleration is balanced by radiative losses.

From Figs. 12 & 13 of Paper I one finds that under the assumed physical conditions the acceleration of the lower energy electrons and positrons typically happens in the regime $\tau_s \gg \tau_d$ while the acceleration of the higher energy leptons happens in the opposite regime.

Thus, assuming for simplicity a power law energy distribution of the relativistic protons $N_p = K_p p^{-s}$, from Eqs.(1), (8), (51), and (53) one finds:

$$p_> = \left(\frac{A_C n_{th} \mathcal{E}_p}{A_w I_o} B^{\omega-1} \right)^{1/(\omega+s-2)} \quad (60)$$

where A_C is the constant in Eq. 1, and

$$A_w = \frac{2(1+\omega+s)}{s-2} \frac{(e/c)^{3-(\omega+s)}}{(\omega+s)^2-1} \left(\frac{p_{low}/m_p c}{em_p} \right)^{2-s} \quad (61)$$

while from Eqs.(2), (8), (49), and (53) one has:

$$p_{max} = \left(\frac{A_{ww}}{A_{rad}} \frac{1}{B_{IC+}^2} \right)^{3/4} \left(\frac{I_o B^{1/2}}{n_{th}} \right)^{1/2}, \quad (62)$$

where A_{rad} is the constant in Eq. 2, $B_{IC+}^2 = B_{IC}^2 + B^2$, and

$$A_{ww} = \frac{3}{5} \pi e^{1/3} \left(\frac{3m_p c^2}{5(\omega-1)} \right)^{2/3}. \quad (63)$$

The number density of the reaccelerated secondary electrons and positrons around p_{max} can be estimated by the integral of the number density of secondary particles injected with $p > p_>$ during the reacceleration stage. From Eqs.(38) (ne-

glecting for simplicity the contributions from the \mathcal{P}_2 and \mathcal{P}_3 terms) and (60), one has :

$$N_{e^\pm}^+ \sim \frac{\Delta_T A(s) c^{-s} \mathcal{P}_1}{s-1} n_{\text{th}} K_p \left(\frac{A_C}{A_{\text{ww}}} \frac{n_{\text{th}} \mathcal{E}_p B^{\omega-1}}{I_o} \right)^{\frac{1-s}{\omega+s-2}}. \quad (64)$$

On the other hand, the number density of electrons with $p \sim p_{\text{max}}$ in the classical secondary model can be obtained from Eqs.(38), (55) and (62) :

$$N_{e^\pm} \sim \frac{p_{\text{max}}^{-(s+1)}}{s-1} \frac{A(s) c^{-s} \mathcal{P}_1}{A_{\text{rad}}} \frac{n_{\text{th}} K_p}{B_{IC+}^2} \quad (65)$$

Thus the increase of the extension of the emitted synchrotron profile (associated to electrons with $p \sim p_{\text{max}} c$) in the secondary–reacceleration model with respect to that in the classical secondary model can be directly estimated from the ratio:

$$N_{e^\pm}^+ / N_{e^\pm} \propto \left(\frac{n_{\text{th}} \mathcal{E}_p B^{\omega-1}}{I_o} \right)^{\frac{1-s}{\omega+s-2}} \left(\frac{I_o B^{1/2}}{n_{\text{th}}} \right)^{\frac{s+1}{2}}, \quad (66)$$

which, in the assumption that $\mathcal{E}_p \propto n_{\text{th}}$, roughly scales as $N_{e^\pm}^+ / N_{e^\pm} \propto n_{\text{th}}^{-1/2} - n_{\text{th}}^{-3/2}$. Eq. 66 provides a simple way to estimate the increase of the extension of the radial profile (at least for $s \sim 2 - 2.3$). However, the injection spectrum of secondary electrons/positrons at lower energies (i.e., $\gamma < 10^3$) is not well described by a simple power law (Eq. 38), and the spectra of protons as affected by reacceleration are not power laws either. Thus a more detailed calculation is required. In Fig. 6 we plot the ratio of the synchrotron emissivities as given with reaccelerated particles and in the context of classical secondary models (the parameters are as used in Fig. 5). It is clear that the models invoking reacceleration of secondary particles may produce broader synchrotron emission with respect to secondary models. However, we also notice that the presence of a cut-off in the synchrotron spectrum as obtained in reaccelerated models (which occurs at lower frequencies with increasing radius) produces a steepening of the synchrotron spectrum which balances the increase of the ratio $J_{\text{Syn}}^+ / J_{\text{Syn}}$ with the distance from the center.

In order to reproduce the extension of the largest radio halos with the assumptions in Sect. 5.1, the synchrotron emissivity in the external regions should be amplified by a factor of ~ 100 with respect to that produced in classical secondary models (e.g., Brunetti 2004, Fig. 2); this large factor is not obtained in our calculations (Fig. 6). In order to obtain a very broad synchrotron radio emission, the radial distribution of the energy density of cosmic ray protons can be forced to be more extended than that of the thermal ICM. However, in this case the synchrotron profile is not broadened enough because at large distances the damping of the Alfvén waves due to cosmic rays gets stronger.

6 DISCUSSION AND CONCLUSIONS

We presented the results of the first self-consistent calculations of the injection and reacceleration of cosmic ray protons and both primary and secondary leptons in the intracuster medium. This goal is reached by solving the coupled equations for the time-dependence of the protons, electrons/positrons and Alfvén waves spectra. The work pre-

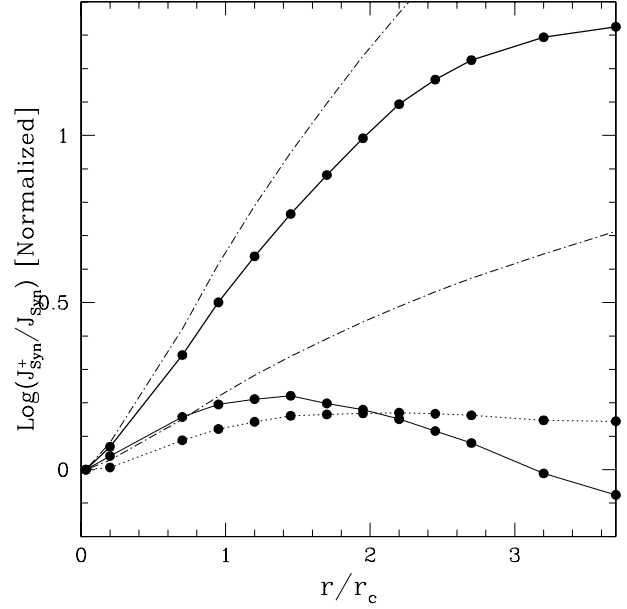


Figure 6. Normalized ratio between the synchrotron emissivity (at 330 MHz) produced by reaccelerated secondary particles, J_{Syn}^+ , and that produced by the stationary injection of secondary particles, J_{Syn} , as a function of the distance from the cluster center (in units of the core radius). The reacceleration models are the same as in Fig. 5 (with the exception of the *hybrid* models shown as dashed lines in Fig. 5) and are shown with the same symbols. The synchrotron emissivity in the classical secondary model is computed in the assumption that $B(r=0) \ll 3\mu\text{G}$. The dot-dashed lines reproduce the behaviour $\propto n_{\text{th}}^{-1/2}$ and $\propto n_{\text{th}}^{-3/2}$ as expected from Eq. 66.

sented here is the natural continuation of a previous work (Brunetti et al. 2004). In particular, in the present paper we illustrate novel results concerning the role of the injection and further re-energization of secondary particles due to their resonant interaction with Alfvén waves. Such secondary particles must exist in the ICM, at least to some extent to be defined: the reason for such a certainty is that we are aware that there are cosmic ray sources in clusters and that the bulk of cosmic rays generated by such sources are diffusively trapped within the ICM (Völk et al. 1996; Berezhinsky, Blasi & Ptuskin 1997). However, neither the amount of energy in the form of cosmic rays, nor their spectrum or their spatial distribution within the ICM are currently known. Their production could be related to the formation of the large scale structure of the universe or to the astrophysical sources within clusters (galaxies and AGNs).

The main assumption of our calculation is the choice of a specific type of MHD waves, namely Alfvén waves. In general one could think of any combination of different modes which behave differently in their interaction with particles (electrons and protons). In particular, the case of magnetosonic waves, considered by Cassano & Brunetti (2005) appears to be particularly interesting since in that case the problem of wave injection on small spatial scales is alleviated. In the present paper, the presence of Alfvén waves on small scales is solved by assuming that fluid turbulence is injected on large scales and gets eventually coupled

with Alfvén turbulence on small scales through the so-called *Lighthill* mechanism. Obviously, direct proofs that this process may be at work require MHD simulations with resolution and dynamical range which are not available at present.

The wave-particle coupling implies a relevant effect on the presence of secondary particles, mainly in two ways: first, the spectrum of parent cosmic rays is changed by the reacceleration process (as also found in Paper I) therefore affecting the spectrum of secondary electrons and positrons. Second, the secondary electrons and positrons are in turn re-energized by the resonant interaction with Alfvén waves. The effect of the reacceleration on the confined cosmic rays is shown in Fig. 1 and most notably consists of a bump at Lorentz factors below $\sim 10^2$, which becomes increasingly more evident with time after the start of the reacceleration phase. At larger Lorentz factors the spectrum of cosmic rays remains unchanged. A similar bump shows in the spectrum of the total population of electrons and positrons (primaries plus secondaries) as plotted in Fig. 3. The pumping of energy into relativistic particles through the resonant interactions with Alfvén waves at some point produces an interesting effect, which in Paper I we named *wave-proton boiler*: the reacceleration of electrons and positrons continues provided the wave damping on the proton component is not too large; when the energy present in the form of protons exceeds some limit the reacceleration of electrons gets suppressed. In this sense the system made of protons, electrons and waves is self-regulated.

One of the most common criticisms to the so-called *reacceleration* scenarios is that the origin of the relic electrons to start with is left as an open issue: we think that the presence of the continuously generated secondary particles largely mitigates this problem, since *pp* interactions continuously inject these particles in the ICM. Moreover, astrophysical sources such as the lobes of radio galaxies and active galaxies are *seen* to pollute the ICM with a population of relativistic electrons, therefore it is plausible that both leptons of primary and secondary origin may be present in a cluster. The secondary particles are expected to be more abundant in the denser central parts of clusters, where the magnetic field is also larger and a correspondingly large contribution to the radio brightness is expected. In the outskirts of the cluster, secondary electrons/positrons are more sparse because of the lower gas density and a dominant primary component should emerge. Therefore the phenomenology of the non thermal activity in a cluster may reasonably be expected to be quite complex. Contrary to the *classical* models of reacceleration of relic primary electrons, the models discussed in this paper do predict that clusters may also be sources of gamma rays both due to the decay of neutral pions and to radiative processes of secondary electrons and positrons, whose spectrum at energies above those at which a reacceleration bump is generated is left basically unchanged.

We applied our calculations to a Coma-like cluster in order to check if the main phenomenological aspects of the non-thermal activity may be reproduced. In doing that we are forced to make the simple assumption that MHD turbulence uniformly fills the cluster volume and that relativistic particles are efficiently mixed with the thermal pool. Clearly more detailed calculations are desirable, possibly making use of next generation numerical simulations.

At variance with standard reacceleration models, in which the source of relic electrons is essentially a free parameter, here the injection of secondary particles is self-regulated by the relativistic hadrons and by the reacceleration process itself, and this increases the predictive power of the model. We find that the synchrotron emissivity at 330 MHz from the core region allows us to infer useful bounds on the energy content in the form of relativistic protons: in general, as illustrated in Fig. 4, observations are hardly explained unless the energy density in cosmic rays at the beginning of the acceleration stage is typically less than about 0.5% of the thermal energy density in the cluster center (at least when both the central brightness and the relatively flat spectral index, $\alpha \sim 0.7 - 0.9$, of the core of Coma C are considered). The rate of injection of energy in the form of Alfvén waves is effectively constrained and depends on the ratio $\mathcal{E}_p/\mathcal{E}_{th}$. For $\mathcal{E}_p/\mathcal{E}_{th}$ larger than a few times 10^{-4} the injection rate is required to be of the order of $\sim 10^{-28} \text{ erg s}^{-1} \text{ cm}^{-3}$ (roughly 2% of the thermal energy during the reacceleration time). A larger rate implies an even lower allowed fraction of cosmic rays in the ICM, while an injection rate significantly smaller would produce a synchrotron spectrum steeper than that observed. Clearly the limits are more stringent when the magnetic field is larger. Similarly these limits are expected to be more stringent when the real injected spectrum of cosmic ray protons is considerably steeper than $s = 2.2$ (adopted throughout the paper) since in this case the back-reaction of protons on the waves is even stronger (Paper I). Finally, for acceleration periods longer than a few 10^8 yrs (adopted in Sect. 5) the limits are expected to be slightly more stringent since in this case the energy budget of protons increases, while the limits on $\mathcal{E}_p/\mathcal{E}_{th}$ would be slightly less stringent for shorter reacceleration stages (provided that they are longer than the typical acceleration time).

We studied in detail how the volume integrated synchrotron spectrum and the radial profile of the radio emission change when the contribution of reaccelerated secondary electrons and positrons is taken into account. The dependence of the results upon the choice of the several parameters involved is illustrated and summarized in Sections 5.3 and 5.4. In principle given viable assumptions the radio emission of Coma (volume integrated spectrum and radial profile) could be explained in terms of reaccelerated secondary electrons and positrons only. In particular, we have shown that the reacceleration of secondary leptons could produce synchrotron profiles which are broader than those expected from the standard acceleration model, although the broadening is still not sufficient to explain the most extended radio halos (at least under the assumptions in Sect. 5). On the other hand the observed, though controversial hard X-ray excess does require an additional component, that can plausibly be associated with primary electrons in the outskirts of the cluster, where secondary particles are not abundant enough.

The possibility to demonstrate the existence of cosmic ray hadrons and secondary electrons/positrons in the ICM is related to the detection of gamma rays due to the decay of the neutral pions and of circular polarization (provided this is not shrouded by the effect of Faraday depolarization in the ICM). In this respect the *Hybrid Models* presented here are qualitatively similar to the secondary models. On the other hand, one way of testing a scenario in which non

thermal radiation is generated by reaccelerated leptons of both primary and secondary origin is to look for a radio tail that should be produced through synchrotron emission of those secondary leptons that are not affected by resonant interactions with Alfvén waves (namely with $\gamma > 10^5$). This radio flux should appear as a sort of recovery of the radio emissivity at high frequency, above the cutoff typical of the reacceleration scenarios. This flux level might be accessible to next generation radio telescopes, such as SKA, provided the radio flux at such high frequencies is not overwhelmingly smaller than the microwave flux at the same frequencies.

In this paper we focus on a specific aspect that is the effect of MHD turbulence on the acceleration of both primary and secondary relativistic particles in the ICM and on the related non-thermal emission from galaxy clusters. If future observations of radio halos will confirm the presence of distinctive features (for example spectral steepenings) which are expected in the case of *in situ* acceleration of the emitting particles, MHD turbulence in the ICM would be unavoidable. In this case, detailed calculations of particle acceleration will be important to indirectly constrain the presence and the properties of the MHD turbulence in the ICM and hopefully its connection with the magnetic field amplification.

In general, turbulence could play a role in several aspects of the physics of the ICM. Large-scale turbulent motions in the ICM may provide a substantial pressure support to the ICM (Kulsrud et al. 1997; Roettiger et al. 1997; Ricker & Sarazin 2001), and in addition to other proposed mechanisms (e.g., Böhringer et al., 2002; Ciotti & Ostriker, 2001), the dissipation of turbulent energy can provide a source of heating to balance the cooling of cluster cores (Fujita, Matsumoto & Wada 2004). The knowledge of the basic aspects of MHD turbulence in galaxy clusters is also crucial to model the transport of heat and metals in the ICM (Cho et al., 2003; Voigt & Fabian 2004).

Future experiments, such as ASTRO-E2 (and NEXT), would hopefully constrain the energy budget associated to the turbulent eddies in the ICM by looking at the profile of the FeK-lines (and other) in the X-ray spectrum of galaxy clusters (Sunyaev et al., 2003).

7 ACKNOWLEDGEMENTS

We acknowledge L.Feretti and the anonymous referee for valuable comments on the presentation of the paper. We acknowledge partial support from MIUR through grant PRIN2004. GB acknowledge partial support from INAF through grant D4/03/15.

REFERENCES

Badhwar G.D., Golden R.L., Stephens S.A., 1977, PhRvD 15, 820
 Barnes A., Scargle J.D., 1973, ApJ 184, 251
 Berezhinsky V.S., Blasi P., Ptuskin V.S., 1997, ApJ 487, 529
 Berezhinsky V.S., Kudriavtsev V.A., 1990, ApJ 349, 620
 Berrington R.C., Dermer C.D., 2003, ApJ 594, 709
 Blasi P., 2000, ApJ 532, L9
 Blasi P., 2004, JKAS 37, 483
 Blasi P., Colafrancesco S., 1999, APh 12, 169

Böhringer H., Matsushita K., Churazov E., Ikebe Y., Chen Y., 2002, A&A 382, 804
 Briel U.G., Henry J.P., Böhringer H., 1992, A&A 259, L31
 Brüggén M., Kaiser C.R., 2001, MNRAS 325, 676
 Brunetti G., 2003, in 'Matter and Energy in Clusters of Galaxies', ASP Conf. Series, 301, p.349, eds. S. Bowyer and C.-Y. Hwang
 Brunetti G., 2004, JKAS 37, 493
 Brunetti G., Setti G., Feretti L., Giovannini G., 2001, MNRAS 320, 365
 Brunetti G., Blasi P., Cassano R., Gabici S., 2004, MNRAS 350, 1174
 Buote D.A., 2001, ApJ 553, L15
 Cassano R., Brunetti G., 2005, MNRAS 357, 1313
 Cavaliere A., Fusco-Femiano R., 1976, A&A 49, 137
 Clarke T.E., Kronberg P.P., Böhringer H., 2001, ApJ 547, 111
 Cho J., Lazarian A., Honein A., Knaepen B., Kassinos S., Moin P., 2003, ApJ 589, L77
 Churazov E., Forman W., Jones C., Böhringer H., 2000, A&A 356, 788
 Ciotti L., Ostriker J.P., 2001, ApJ 551, 131
 Dennison B., 1980, ApJ 239L, 93
 Dermer C.D., 1986a, A&A 157, 223
 Dermer C.D., 1986b, ApJ 307, 47
 Dogiel V.A., 2000, A&A 357, 66
 Dolag K., Ensslin T.A., 2000, A&A 362, 151
 Drury L., 1983, SSRv 36, 57
 Eilek J.A., 1979, ApJ 230, 373
 Eilek J.A., Henriksen R.N., 1984, ApJ 277, 820
 Eilek J.A., Weatherall J.C., 1999, in 'Diffuse Thermal and Relativistic Plasma in Galaxy Clusters', MPE Report 271, eds. H. Böhringer, L. Feretti, P. Schuecker
 Ensslin T.A., 2004, JKAS 37, 455
 Ensslin T.A., Lieu R., Biermann P.L., 1999, A&A 344, 409
 Fabian A.C., Sanders J.S., Ettori S., Taylor G.B., Allen S.W., et al., 2000, MNRAS 318, L65
 Feretti L., 2003, in 'Matter and Energy in Clusters of Galaxies', ASP Conf. Series, 301, p.143, eds. S. Bowyer and C.-Y. Hwang
 Fujita Y., Takizawa M., Sarazin C.L., 2003, ApJ 584, 190
 Fujita Y., Matsumoto T., Wada K., 2004, ApJ 612, L9
 Fusco-Femiano, R., Dal Fiume, D., Orlandini, et al., 2003, in 'Matter and Energy in Clusters of Galaxies', ASP Conf. Series, 301, p.109, eds. S. Bowyer and C.-Y. Hwang
 Fusco-Femiano, R., Orlandini, M., Brunetti G., et al., 2004, ApJ 602, L73
 Gabici S., Blasi P., 2003, ApJ 583, 695
 Giovannini G., Feretti L., Venturi T., Kim K.-T., Kronberg P.P., 1993, ApJ 406, 399
 Govoni F., Ensslin T.A., Feretti L., Giovannini G., 2001, A&A 369, 441
 Jaffe W.J., 1977, ApJ 212, 1
 Kato S., 1968, PASJ 20, 59
 Kulsrud R.M., Ferrari A., 1971, Ap&SS 12, 302
 Kulsrud R.M., Cen R., Ostriker J.P., Ryu D., 1997, ApJ 480, 481
 Lacombe C., 1977, A&A 54, 1
 Landau L.D., Lifshitz E.M., 1959, *Fluid Mechanics*, Pergamon Press, Oxford
 McNamara B.R., Wise M., Nulsen P.E.J., David L.P., Sarazin C.L., et al., 2000, ApJ 534, L135
 Melrose D.B., 1968, ApSS 2, 171
 Miller J.A., Roberts D.A., 1995, ApJ 452, 912
 Miniati F., Jones T.W., Kang H., Ryu D., 2001, ApJ 562, 233
 Moskalenko I.V., Strong A.W., 1998, ApJ 493, 694
 Ohno H., Takizawa M., Shibata S., 2002, ApJ 577, 658
 Petrosian V., 2001, ApJ 557, 560
 Reimer A., Reimer O., Schlickeiser R., Iyudin A., 2004, A&A 424, 773
 Rephaeli Y., Gruber D., 2003, ApJ 595, 137
 Ricker P.M., Sarazin C.L., 2001, ApJ 561, 621

- Roettiger K., Loken C., Burns J.O., 1997, ApJ 109, 307
Rossetti M., Molendi S., 2004, A&A 414, L41
Ryu D., Kang H., Hallman E., Jones T.W., 2003, ApJ 593, 599
Sarazin C.L., 1999, ApJ 520, 529
Sarazin C.L., 2002, in *Merging Processes of Galaxy Clusters*, Eds. L.Feretti, I.M.Gioia, G.Giovannini, ASSL, Kluwer Ac. Publish., p. 1
Sarazin C.L., Kempner J., 2000, ApJ 553, 73
Schlickeiser R., 2002, *Cosmic Ray Astrophysics*, Springer-Verlag, Berlin Heidelberg
Schlickeiser R., Miller, J.A., 1998, ApJ 492, 352
Schuecker P., Böhringer H, Reiprich T.H., Feretti L., 2001, A&A 378, 408
Stecker F.W., 1970, Ap&SS 6, 377
Stephens S.A., Badhwar G.D., 1981, Ap&SS 76, 213
Sunyaev R.A., Norman M.L., Bryan G.L., 2003, Astr. Letters 29, 783
Tsytovich V.N., 1972 *An Introduction to the Theory of Plasma Turbulence*, Pergamon Press.
Voigt L.M., Fabian A.C., 2004, MNRAS 347, 1130
Völk H.J., Aharonian F.A., Breitschwerdt D., 1996, SSRv 75, 279
Yan H., Lazarian A., 2004, ApJ 614, 757
Zhou Y., Matthaeus W.H., 1990, J.Geophys.Res. 95, 14881